Properties of graphite composites based on natural and synthetic graphite powders and a phenolic novolac binder

P.P. Magampa[1], N. Manyala[2], W.W. Focke[3,*]

[1]SARChI Chair in Carbon Materials and Technology, Institute of Applied Materials, Department of Chemistry, University of Pretoria, Private Bag X20, Hatfield 0028, South Africa
[2]SARChI Chair in Carbon Materials and Technology, Institute of Applied Materials, Department of Physics, University of Pretoria, Private Bag X20, Hatfield 0028, South Africa
[3]SARChI Chair in Carbon Materials and Technology, Institute of Applied Materials, Department of Chemical Engineering, University of Pretoria, Private Bag X20, Hatfield 0028, South Africa

Abstract

Model graphite composites, similar to those used in nuclear applications as encasement material in fuel pebbles, were prepared by uniaxial cold compression moulding. They contained natural flake graphite, synthetic graphite and 20 wt.% phenolic novolac resin binder. The materials were carbonised at 900 °C in a nitrogen atmosphere and then annealed at 1800 °C in helium atmosphere. The X-ray diffraction studies showed that the graphite in these composites had hexagonal crystal structure after annealing. Raman spectroscopy revealed the presence of the structurally disordered phase derived from the carbonised resin. Optical microscopy revealed a flake-like microstructure for composites containing mainly natural graphite and needle-coke like particles for composites containing mainly synthetic graphite. The composites featured anisotropic property behaviour as the particles were partially aligned in a direction perpendicular to the compression direction. Thermogravimetric analysis studies showed that the annealed graphite composites were stable in air to 650 °C. The linear thermal expansion coefficients measured by thermomechanical analysis (20-600 °C) in the direction of pressing were in the range 5 to 9×10^{-6} K^{-1} and in the range $1.2\text{-}2\times10^{-6}$ K^{-1} in the direction normal to pressing. The thermal conductivity of the composites were measured using Xenon flash method from 100 to 1000 °C and the values ranged from 19 to 30 $W.m^{-1}.K^{-1}$.

Key words: Fabrication, microstructure, thermal properties

*Corresponding author: Tel: +27 12 420 3728; fax: +27 12 420 2516; e-mail: walter.focke@up.ac.za

1. Introduction

The Pebble Bed Modular Reactor (PBMR) is a high temperature graphite-moderated nuclear reactor that uses helium as a coolant. The triple coated (TRISO) particles contain the enriched

uranium oxide fuel. The coatings comprise layers of various forms of pyrolytic carbon and silicon carbide [1, 2]. They are designed to retain any fission products released at the elevated reactor operating temperatures [3, 4]. Large numbers of the TRISO particles are embedded in the matrix of each of the spherical graphite pebbles. These graphite composites are moulded from a compound containing natural flake graphite (64 wt.%), synthetic graphite (16 wt.%) and a phenolic resin binder (20 wt.%). The moulded spheres are heat-treated to 1800 °C to convert the binder into a glassy carbon that provides structural integrity. It also acts as a moderator material, slowing down the speed of neutrons to thermal levels so that the fission reactions can occur. The graphite composite must possess suitable properties e.g., very low impurity levels, density exceeding 1.7 g cm^{-3}, high thermal conductivity, high mechanical strength, high stability under irradiation, high oxidation resistance and low thermal expansion coefficient [5].

Similar compositions have been used in other high temperature reactors [4] and were judged to be provide the required properties. However, little was reported about the relationship between the fabrication/processing method, the resulting microstructure and the final properties that can be achieved. For example, what is the microstructure of the composites? What is the spatial arrangement of the graphite fillers? What is the effect of changing the relative proportions of graphite fillers in the matrix? How are properties affected when lower density materials are fabricated? In this study, fuel-free low-density graphite composites were prepared. The relative proportion of the two graphite fillers was varied keeping the phenolic

Table 1: Green state composition and physical properties of carbon-graphite composites annealed (in a He atmosphere) at 1800 °C for 2 h.

Property	**Units**	**Composition NG:SG:novolak resin**			
Composition	**wt.%**	**0:80:20**	**40:60:20**	**64:16:20**	**80:0:20**
d-spacing	Å	3.371	3.370	3.371	3.364
Open porosity	%	41.9	33.6	31.5	27.6
Helium density	kg m^{-3}	2130±0.5	2068±0.5	2091±0.9	2095±0.9
Bulk density	kg m^{-3}	1238±3	1372±2	1432±4	1516±4
$CTE_{\perp}\times10^{-6}$	K^{-1}	6.25±0.89	5.82±0.75	9.58±1.61	7.58±0.71
$CTE_{\parallel}\times10^{-6}$	K^{-1}	2.06±0.50	2.08±0.44	1.94±0.53	1.91±0.45
$CTE_{\perp}/CTE_{\parallel}$	-	3.0	2.8	4.9	4.0
Bending strength	MPa	8.61±0.59	4.96±1.26	10.2±2.1	-
Bending modulus	GPa	2.06±0.39	1.21±0.35	1.69±0.27	-

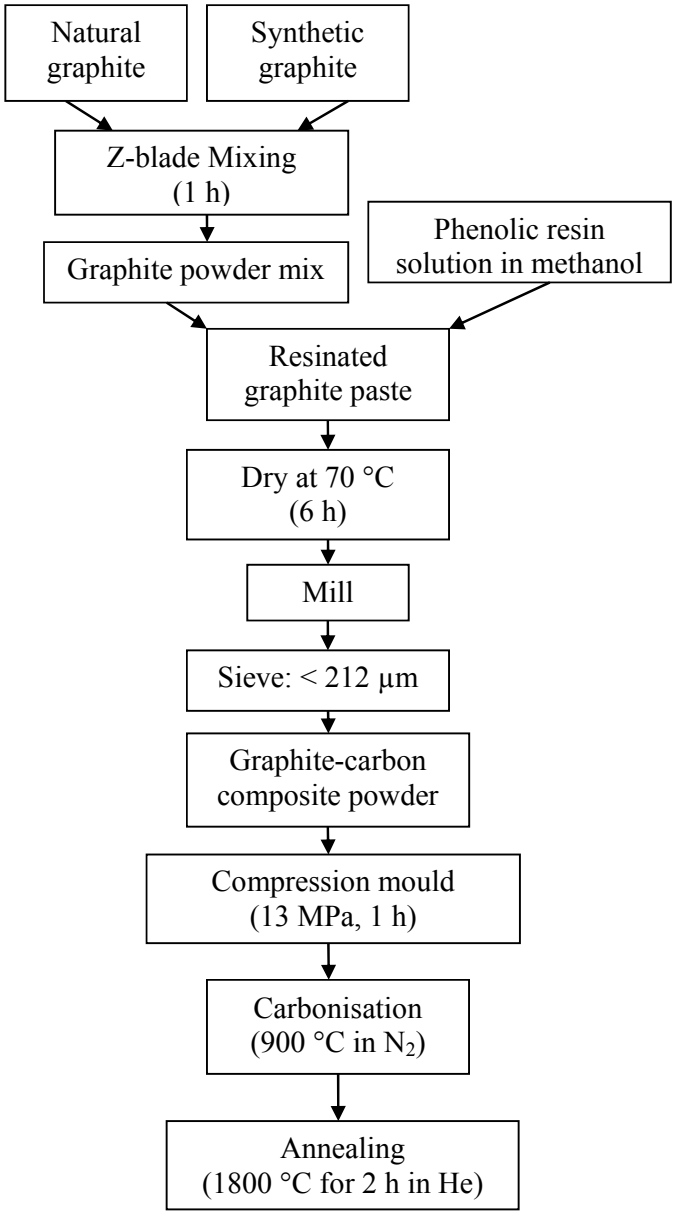

Figure 1: Fabrication scheme for the graphite-phenolic resin composites.

resin binder content fixed. The microstructure was studied and the thermal and mechanical properties were determined in an attempt to answer, at least in part, some of these questions.

2. Material and methods

Graphite composites containing a fixed amount of phenolic resin binder (20 wt.%) were fabricated according to the procedure outlined in Figure 1. The compositions of the graphite composites tested are shown in Table 1. They were labelled according to the proportions of

natural flake graphite, synthetic graphite and novolac binder in wt.%. For example, the composite containing 64 wt.% natural graphite, 16 wt.% synthetic graphite and 20 wt.% phenolic resin was labelled 64:16:20, etc.

The natural flake graphite and the synthetic graphite powder were mixed in a Z-blade mixer (Jones Mixers, South Africa) for one hour. A methanol solution of the phenolic novolac resin

was then added. Just sufficient methanol was used to ensure a flowable paste. This resinated paste was dried at 70 °C for 6 h in a convection oven. The resulting rigid residue was then ground into a powder using a carbon steel ring mill and sieved through 212 μm mesh using electromagnetic shakers (Labotec, South Africa). About 120 g sieved powder was placed in a 100 mm ϕ cylindrical stainless steel die. Disc-shaped test specimens were compression moulded for 1 h at 13 MPa in a hydraulic press (Vertex Automation Pty (Ltd)). The green moulded specimens were then carbonised at 900 °C in N_2 atmosphere to remove all volatiles. This was followed by an annealing step at 1800 °C in a helium atmosphere using a graphitising furnace (Thermal Technology Inc., USA). The samples were maintained at this temperature for 2 h and then allowed to cool to ambient conditions. Depending on the measurement to be made, the samples were cut to the required dimensions with an Isomet 4000 linear precision diamond saw (Buehler, Germany).

3. Experimental

3.1 X-ray diffraction (XRD)

The diffraction patterns of the annealed graphite composite powders were recorded using a BRUKER's D8 ADVANCE powder diffractometer. Measurements were done using CuKα radiation (0.15418 nm) with the generator operated at 40 kV and 40 mA. Detection of the diffracted beam was done using 1 D Position Sensitive Detector (Lynx eye detector). Measurements were performed in the range 15° to 90° in 2θ with a of 0.04° step size and a counting time 0.2 s. Phase identification was done using EVA's Diffrac^{plus} Basic evaluation Package SEARCH & MATCH in conjunction with ICCD 2007 PDF-2 database. The interlayer spacing, d_{002} was calculated using the Bragg equation.

3.2 Raman analysis

The Raman spectra were recorded with the T64000 series II triple spectrometer system from HORIBA Scientific, Jobin Yvon Technology using the 514.3 nm laser line of a coherent Innova®70 Ar^+ laser with a resolution of 2 cm^{-1} in the wavenumber range 1200 to 1750 cm^{-1}. The samples were recorded in a backscattering configuration with an Olympus microscope attached to the instrument (using a LD 50× objective). A liquid nitrogen-cooled CCD detector was used with a laser power of 6 mW at the sample. The accumulation time was 120 s and the spectra were baseline corrected with the LabSpec software program. All the spectra were collected at a spot scale of 2 μm.

3.3 Optical microscopy (OM)

The microstructure of the raw graphite samples and heat-treated moulded graphite composites was studied by optical microscopy (OM) under reflected and polarised light. A Leica DM 2500 M microscope was used. The samples were mounted in an epoxy resin. They were polished with a Buehler Alpha 2 speed grinder-polisher with a continuous flow of water for 1 min for each of the silicon carbide grinding papers (400, 600, 1200 grits). The samples were then successively polished with Buehler Metadi polishing suspensions of size 1.0 μm and 0.05 μm. This was done for 3 and 5 min, respectively. This polishing methodology yielded a very smooth sample surfaces.

3.4 Scanning Electron Microscopy (SEM)

The SEM images were obtained using an ultrahigh resolution field emission SEM (HR FEGSEM Zeiss Ultra Plus 55) with an InLens detector at an acceleration voltage of 2 kV.

3.5 Pycnometry

The bulk density of the pre-weighed moulded annealed graphite composites was measured using a Geopyc 1360 pycnometer. The Helium density was measured with Accupyc II 1340 V1.03 Helium pycnometer. The volume of the sample cup was calibrated prior to analysis by filling it with helium gas until it reached a pressure of 134.45 kPa. This was done in 5 cycles. After calibration with standard steel balls, the pre-weighed sample was placed in the sample chamber and filled with helium gas until a pressure of 134.45 kPa was reached. The sample volume, excluding closed pores in the sample, was measured. Triplicate measurements were performed per sample and three samples were measured per type. Their average was used for

calculating helium density. Both pycnometers were purchased from Micromeritics Instruments Corporation, USA. The open accessible porosity percentage in the annealed graphite composites were calculated using equation (1) below:

$$\text{Open porosity} = \left(1 - \rho_B / \rho_{He}\right) \times 100\,\% \quad (1)$$

where ρ_B is the bulk density and ρ_{He} is the helium density both in kg m^{-3}.

3.6 Thermogravimetric analysis (TGA)

The air oxidation behaviour of the powdered raw graphite samples, the phenolic resin and the annealed graphite composites was determined by TGA analysis using a Mettler Toledo A851 TGA/SDTA machine. About 20 mg samples were placed in a 70 μL alumina pan and heated from 18 to 1000 °C at a scan rate of 5 °C/min in instrument grade air flowing at 50 mL/min.

3.7 Thermomechanical (TMA) analysis

The linear coefficients of thermal expansion (CTE) of the annealed solid graphite composites were determined in expansion mode with a TA Instruments TMA Q400 V22.1 analyser. The runs were made on a quartz stage from 20 to 1000 °C at a heating rate 5 °C/min in N_2 flowing at a rate 50 mL/min and applying a force of 0.02 N. The expansion measurements were recorded along the uniaxial pressing direction of the compacts and in the direction normal to pressing direction. The dimensions of the samples used were 10 mm × 5 mm × 5 mm. The instantaneous thermal expansion coefficient, CTE, was calculated as follows:

$$\text{CTE} = \frac{1}{L_0}\frac{\partial L}{\partial T} \quad (2)$$

where L is the length of the sample in m, T is the temperature in K, and L_0 is the initial length of the sample in m at some initial temperature T_0 [6]. The instrument was calibrated using a copper sample with known linear CTE (17×10^{-6} K^{-1}). Measurements were done both parallel (∥) and perpendicular (⊥) to the direction of the pressing force.

3.8 Thermal conductivity from Xenon flash photolysis

The thermal conductivity of the annealed graphite composites samples were measured using the Xenon flash method. The thermal diffusivity were measured at each temperature using the

Clark and Taylor analysis of a back face thermogram generated from a Xenon flash on the front face [7]. Samples of 20 mm in diameter and 2 mm in thickness were used in an Anter Flashline 3000 with a Xenon flash under nitrogen flow. A thermographite sample was used as a reference. The thermal conductivity of the samples was calculated from measured thermal diffusivity, density and specific heat of the samples at each temperature using the following equation:

$$k = \alpha \rho C_p \quad (3)$$

where k is the thermal conductivity in W m^{-2} K^{-1}, α is the thermal diffusivity in m^2 s^{-1}, ρ is the density in kg m^{-3} and C_p is the specific heat in J kg^{-1} K^{-1}.

3.9 Mechanical properties via four-point bending tests

Rectangular annealed graphite composite samples were cut to the specifications of ASTM Standard C651-91 (Reapproved 2000). The length of the samples were 40.00±0.02 mm, their widths were 10.00±0.02 mm and had thickness of 5.00±0.02 mm. The samples were polished on their faces with 1200 silicon carbide paper grit to make them smooth and free of visible defects. The samples were loaded onto a tensile tester (LRX plus tensile tester, LLOYD Instruments); the support and loading spans used were 30 and 10 mm, respectively. A loading rate of 1 mm/min was utilised. All samples tested were unnotched. The flexural strength was calculated using the following equation:

$$\sigma = \frac{F L}{b d^2} \quad (4)$$

where σ is the flexural strength in Pa, F is the load (force) in N at fracture, L is the length of the support span in m, b and d are the width (m) and thickness (m) of the sample, respectively. At least triplicate measurements were performed for each composition.

4 Results and discussion

4.1 Fabrication

The moulded graphite composites discs of diameter 100 mm were successfully fabricated. Pressing the graphite powders individually or as mixtures without the binder did not yield monolithic structures. Thus the incorporation of the phenolic resin binder is essential. Cunningham et al. [8] previously noted similar behaviour for such graphite composites

although they employed a lower binder level (10 wt.%). Addition of the phenolic resin in the form of a methanol solution ensured a more uniform distribution of the resin in the graphite powder than would have been possible by dry solid addition. The milling of the dried samples also aided, to some extent, homogeneous distribution of the binder resin and graphite powder particles.

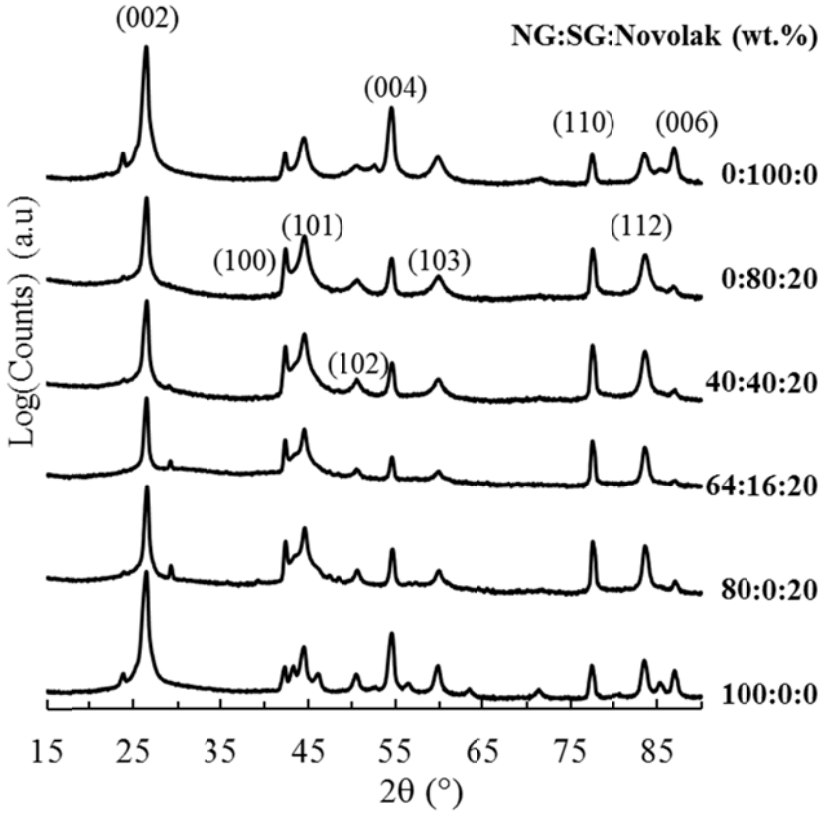

Figure 2: The X-ray diffraction patterns of raw graphite powders and solid annealed graphite-resin composites of various compositions heat-treated to 1800 °C in a helium atmosphere.

4.2 X-ray diffraction (XRD) analysis

The X-ray diffraction patterns of the as-received graphite powders and the solid annealed graphite composites are shown in Figure 2. The patterns for all the annealed composites, as well as the synthetic graphite (SG), were consistent with the hexagonal crystalline phase of graphite [9]. The natural graphite (NG) pattern corresponded to the graphite-3R pattern which contains both the hexagonal and rhombohedral crystalline phases. The latter phase possesses additional peaks at 2θ = 43.4, 46.2 and 56.6° [10]. It is well known that the hexagonal phase

is the more stable phase and that the rhombohedral phase is thermodynamically unstable. The presence of the latter phase in the natural graphite could have been caused by the milling operation used during its comminution. The rhombohedral phase results from stacking faults of the hexagonal phase [11, 12]. Owing to an annealing effect, this phase did not appear in the profiles of the heat-treated composites (especially those containing mainly natural graphite and binder [11]. All the composites showed a hexagonal crystal graphite structure after annealing. The reflection at $2\theta \approx 30°$ could not be assigned but may be an instrumental artefact. This reflection did not appear in the patterns of the raw graphite samples or in the annealed graphite composite powders (not shown here).

Table 1 lists the interlayer spacing values, d_{002}, obtained from the X-ray diffraction measurements. The average interlayer spacing of the raw natural flake and synthetic graphite samples were 0.3357 nm and 0.3354 nm, respectively. Thus the raw graphite powders featured interlayer spacing values close to that of the ideal single crystal graphite [13]. The annealed graphite composites showed larger average interlayer spacing (i.e. 0.3364 nm to 0.3371 nm) than the raw graphite powders. This is attributed to defects introduced during the milling of the green compound and the high pressure moulding process used to make the samples.

4.3 Raman spectroscopy

The Raman spectra, shown in Figure 3, exhibit two distinct peaks. The disorder induced Defect 'D' band is located at approximately 1350 cm^{-1} and the structural order induced Graphite 'G' band at approximately 1580 cm^{-1}. The intensity ratio of the 'D' peak (I_D) to the 'G' peak (I_G) provides an indication of the degree of structural ordering in the carbon material. Pure crystalline graphite features a very low intensity D-peak and the intensity ratio is close to zero [14-16]. The Raman spectrum of neat phenolic resin did not show any Raman peaks. The Raman spectrum (not shown) for the carbonised resin confirms it is non-graphitic and highly disordered. The estimated intensity ratios of the synthetic graphite, natural graphite, and carbonised resin were 0.12, 0.18, and 0.9 respectively. Therefore the degree of structural ordering followed the order: Carbonised resin < Natural graphite < Synthetic graphite.

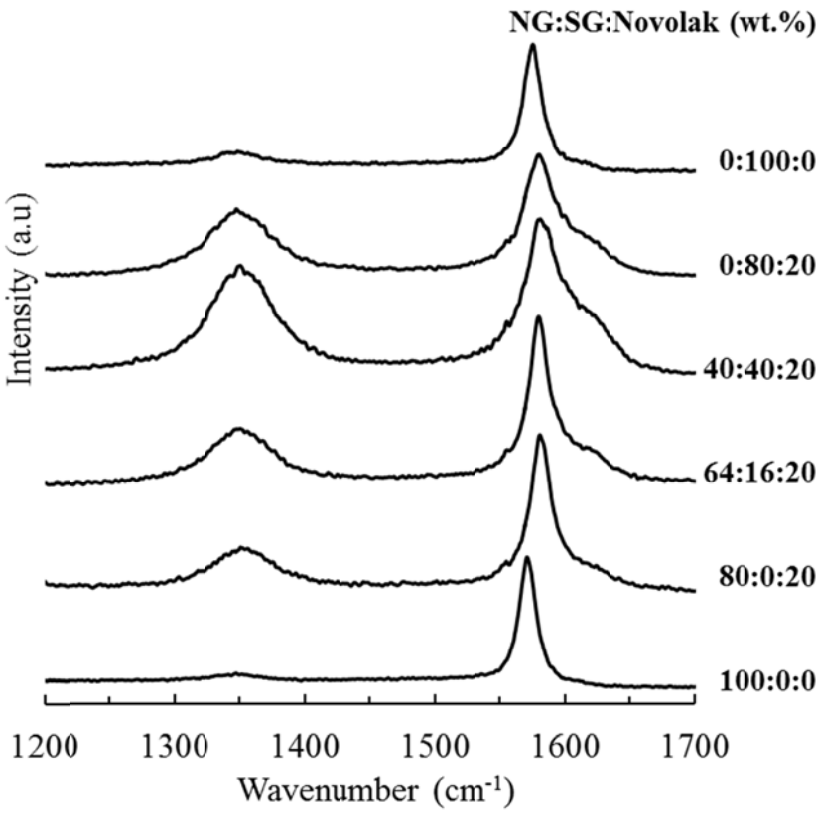

Figure 3: The Raman spectra of the neat graphite precursors and annealed carbon-graphite composites.

The disorder in the raw natural graphite could be due to the presence of impurities or the rhombohedral crystal forms. The Raman spectra of the annealed graphite composites are also shown in Figure 3. The annealed graphite composites showed more intense and broader 'D' peaks than the raw graphite powders. This is due to the presence of the highly disordered carbon residue derived from the resin binder and, to a lesser extent, due to defects induced during the milling of the samples. The intensity ratio for the composite containing only synthetic graphite and binder, i.e. 0 wt.% NG, is 0.59 while the one containing natural graphite and binder, i.e. 80 wt.% NG, is 0.37. Thus the incorporation of the resin and subsequent milling resulted in more structural defects in the synthetic graphite composite than in the other composites. This is surprising as, according to the XRD and Raman results, the raw natural graphite powder was less perfect than the synthetic one. However these results suggest that annealing improved the perfection of the natural graphite.

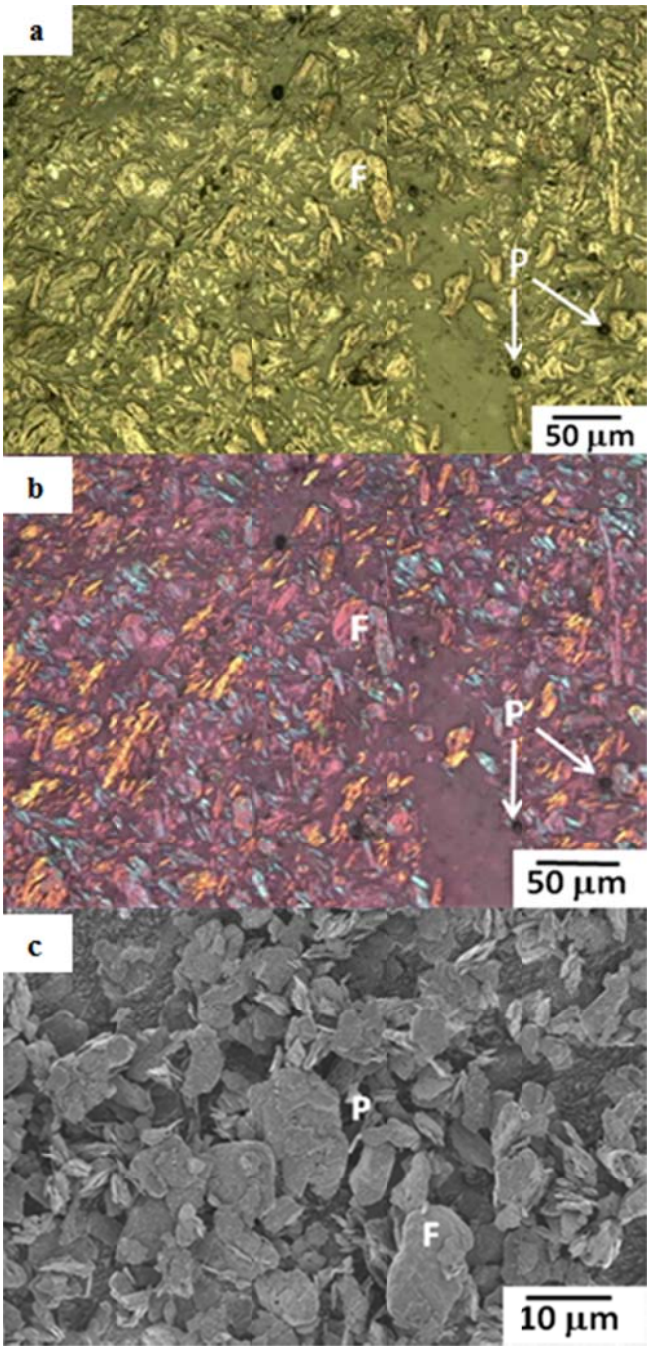

Figure 4: The micrographs of raw natural graphite under: (a) reflected light, (b) polarised light and (c) SEM image.

4.4 Optical microscopy (OM) analysis

The reflected light, polarised light and scanning electron micrographs of the raw natural graphite are shown in Figure 4(a), 4(b) and 4(c), respectively. The reflected light micrograph shows that the natural graphite consists of flake-like particles (F) of different sizes with some pores (P) observed within the particles. Under polarised light microscopy, see Figure 4(b), the

grains within particles show different interference colours due to the interaction of their basal planes with incident polarised light [17]. Grains that appear yellow or blue are aligned perpendicular to each other. The grains at intermediate angles appear pink while the mounting-resin appears purple. The scanning electron micrograph of the natural graphite shown in Figure 4(c) clearly shows a flake-like morphology at higher magnification. The microstructure of the synthetic graphite is different from that of the natural graphite. The reflected and polarised light micrographs are shown in Figure 5(a) and 5(b), respectively; it consists of thin needle-coke particles (NC) and some fine grained particles (FG). The SEM image as shown in Figure 5(c) shows that the particles are more compact relative to the natural graphite powder.

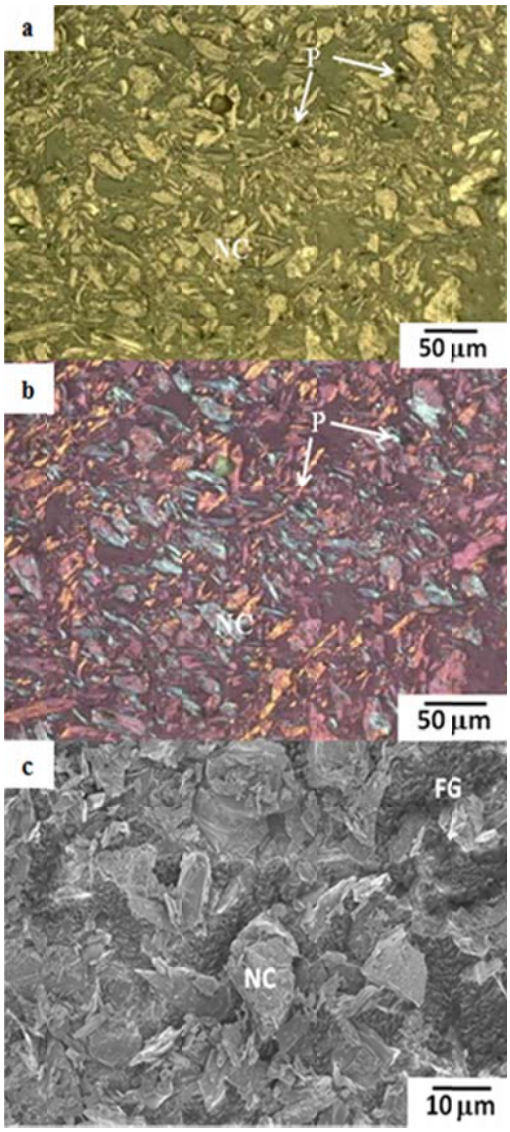

Figure 5: The micrographs of raw synthetic graphite under: (a) reflected light, (b) polarised light and (c) SEM image of the synthetic graphite.

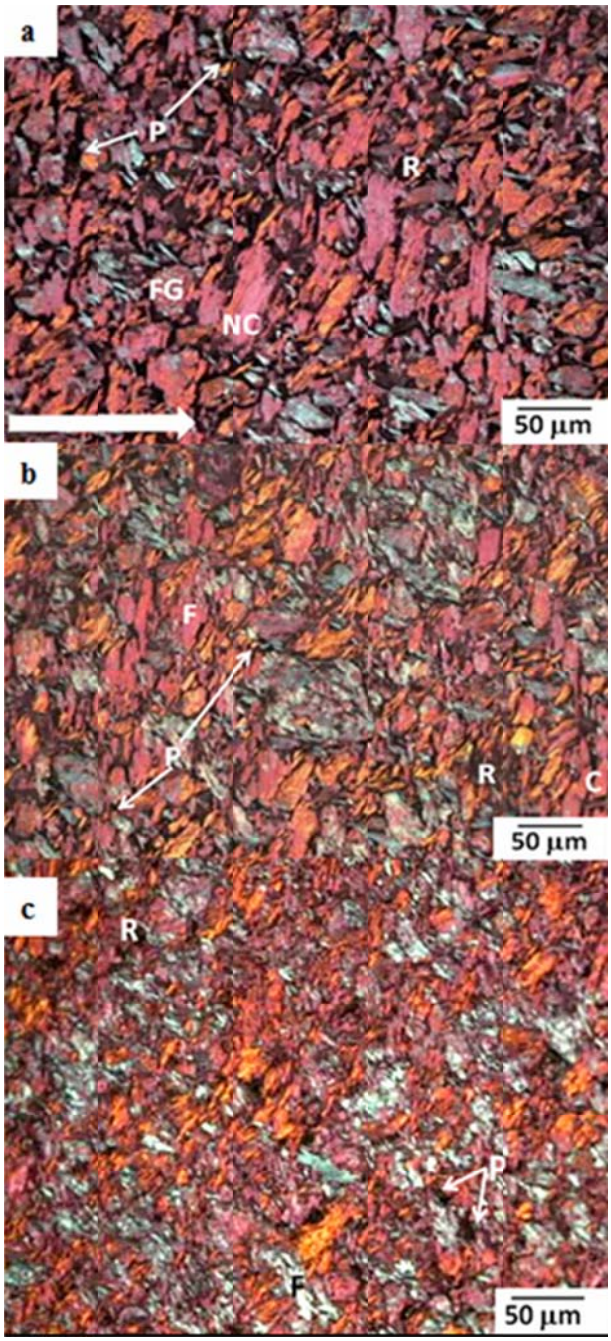

Figure 6: The polarised optical micrographs of annealed (1800 °C) graphite composites: (a) 0 wt.% NG, (b) 40 wt.% NG and (c) 64 wt.% NG. All contained a fixed amount of binder (20 wt.%)

The polarised light micrographs of annealed graphite composites containing various compositions are shown in Figure 6. The micrograph shown here were taken in the direction perpendicular to pressing (the white arrow shown in Figure 6(a) shows the pressing direction). Clearly the annealed graphitic composites comprised compacted particles relative to the raw graphite powders due to the pressing operation and the binding effect of the resin.

A composite containing only synthetic graphite and binder, see Figure 6(a), showed a microstructure having compacted needle-coke particles (NC) and fine grained (FG) mosaics inherent from the synthetic graphite. The resin-derived carbon (R) appears blurry under polarised light because it is optically non-textured. Pores (P) were also observed, this porosity result from volatilization of the phenolic resin during heat-treatment. The graphite particles themselves appear to be partially aligned at an angle perpendicular to the pressing direction.

However, the microstructure of the composite containing equal amounts of the graphite powders, see Figure 6(b), appears more flake-like and it is challenging to distinguish individual particles from the respective graphite particles in this micrograph. The composite containing mostly natural graphite and binder, Figure 6(c), showed more compacted flake-like particles and appeared to be less porous than the other compositions although they were pressed at the same pressure for equal duration. These micrographs support preferential orienting of the flakes in the direction normal to pressing. However, the crystallites within the particles could be oriented differently.

4.5 Pycnometry

The open porosity of the annealed graphite composites was quantified by pycnometry. This crucial parameter affects properties such as thermal expansion and oxidative stability. The bulk and helium densities of the annealed graphite composites are presented in Table 1. The bulk density increased as the natural graphite content increased. The helium density of the annealed carbon-graphite composites agreed with each other to within 1.6 %. It is worth noting that the measured helium densities of the composites were also very close to the expected theoretical densities. The latter were calculated from the weight fractions and densities of the raw graphite powders and carbonised resin. The open porosity, calculated using equation (1), decreased with the increase in the amount of natural graphite content in the composite. This is consistent with the microstructural observation that the composite containing no natural graphite appeared more porous (see Figure 6(a)). The decrease in open porosity as the natural graphite increases could be attributed to the malleability of the natural graphite flakes particles. During the pressing operation they deformed more readily to form denser compact structures. The average open porosity of the composites was approximately 28 %.

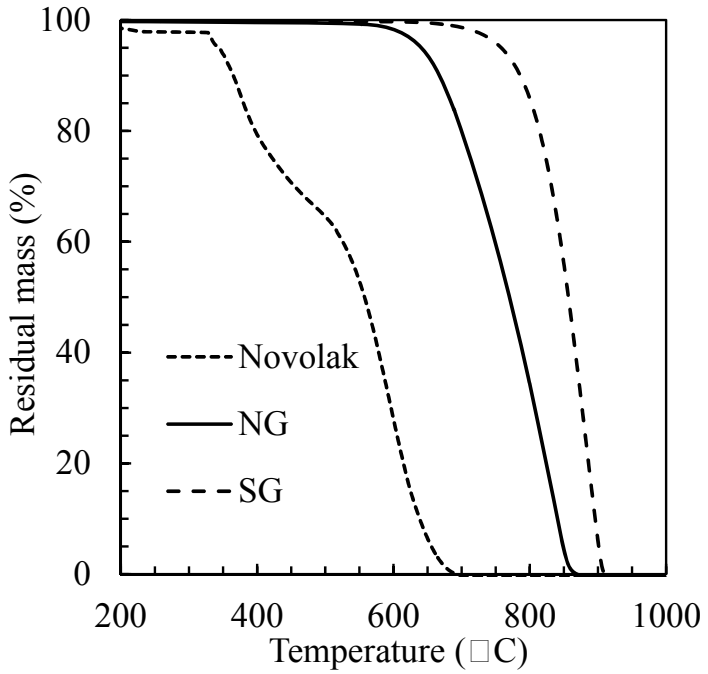

Figure 7: TGA profiles of the phenolic resin, natural graphite and synthetic graphite heated at 5 °C/min in air.

4.6 Thermogravimetric (TG) analysis

The oxidative stability of the raw materials (graphite powders and resin) in air, as well as that of the annealed graphite composites, was studied by thermogravimetric analysis. The TGA profiles of the phenolic resin, natural graphite and synthetic graphite are shown in Figure 7. The onset (T_i) and endset (T_e) air oxidation temperature were determined using intersection of the segments before and after inflection points [18]. The temperature at which the sample loses maximum weight is denoted T_m. The neat phenolic resin had a lower stability than the other raw materials. It started to lose mass at a T_i value of approximately 120 °C due to the loss of moisture, followed by loss of volatiles in the temperature range 340-510 °C. The loss of carbonaceous matter was observed above 510 °C and the endset air oxidation was reached at a T_e of about 700 °C. The weight losses associated with moisture, volatiles and resin carbon oxidation were 0.89%, 31.4% and 67.2%, respectively. The phenolic resin had an ash content of 0.5%. The derivative weight loss curves of the phenolic resin (not shown) revealed that mass loss occurred in five steps with the maximum mass loss rate observed at about 631 °C. The natural graphite was less reactive than the phenolic resin as it started to oxidise at higher temperatures, i.e. about 600 °C. The endset oxidation temperature (T_e) of the natural graphite was about 860 °C. The TG profile of the synthetic graphite showed that it was most

stable against oxidation with a T_i value of about 750 °C and the T_e of about 900 °C. The graphite powders contained negligible ash. The lower onset temperature of the neat natural graphite can be attributed to the presence of catalytic impurities such as Fe and Na in the sample [19]. The heat-treatment at 1800 °C is expected to partially deactivate these impurities. In addition, the raw natural graphite had structural defects (rhombohedral crystalline phase as evidenced by XRD) which made them more susceptible to oxidation. These observation are consistent with reports in literature [20] that air oxidation of carbonaceous materials depend on parameters such as crystal structure and surface area. The bimodal response in the DTG curves (not shown) indicated that the oxidation of natural graphite proceeded in two overlapping steps. In contrast, oxidation of the synthetic graphite was a single-step reaction. The SEM image of the natural graphite in Figure 4(c) showed the sample to be more porous than that of the synthetic graphite, see Figure 5(c), this could also be one of the reasons why the natural graphite was more reactive in air. The air oxidative stability of the synthetic graphite could also be related to how it was made especially if it was somewhat purified. Another important point is that the natural graphite had a mean particle size of 30 μm while that of the synthetic graphite was about 49 μm, this also contributed to lower reactivity in air for the synthetic graphite. It is well known that the larger the average particle size, the more resistant to air oxidation the graphitic material becomes [21, 22].

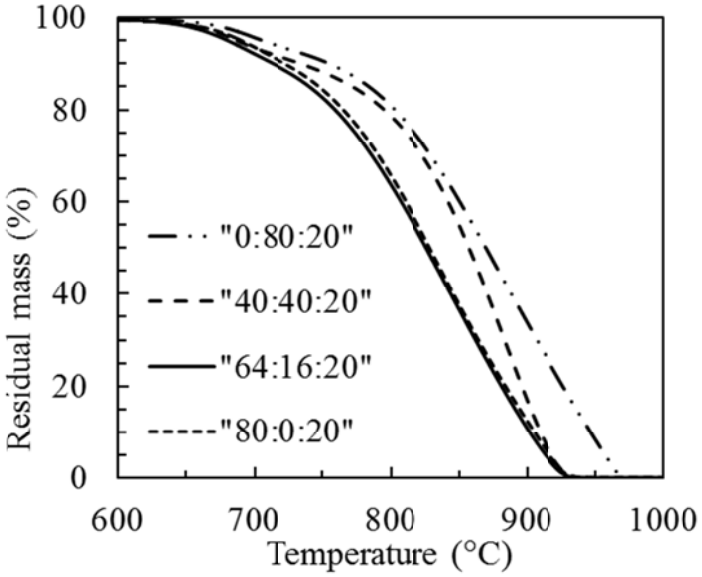

Figure 8: The TGA profiles of the annealed graphite composites heat-treated to 1800 °C (in a helium atmosphere) at 5 °C/min in air and soaked for 2 hours.

The TG profiles of the annealed graphite composites are shown in Figure 8. These composites showed pronounced air oxidation stability with an onset temperature (T_i) at

approximately 650 °C. The endset oxidation temperature (T_e) of these composites was ca. 940 °C. However the composite containing only synthetic graphite and binder showed slightly higher onset and endset air oxidation temperatures, i.e. about 670 and 980 °C, respectively. The lower reactivity of the annealed composites in air is attributed to the heat-treatment which annealed some structural defects and deactivated catalytic impurities especially in the composites containing mainly natural graphite as a major component (i.e. 64% and 80% NG). These composites were observed to be oxidatively less stable than the other composites (i.e., 0% and 40% NG) but the difference was about 50 °C. The mass loss rate curves for the annealed samples appeared bimodal. The first step around 700 °C was due to the loss of resin-derived carbon which oxidises first, followed by loss of graphitic carbon around 850 °C. The loss of resin-derived carbon appeared to wane with increasing natural graphite content. The reason for this is not understood at this point. These graphitic composites were oxidatively stable below 650 °C and therefore in the absence of air, thermal gradients and high neutron fluxes, they should be able to withstand high temperature reactor conditions.

4.7 Thermomechanical (TMA) analysis

The linear expansion behaviour of the annealed graphite composites was studied using thermomechanical analysis. The annealed composites expanded linearly and uniformly in the temperature range 100 to 600 °C. All the annealed graphite composites showed approximately constant α_P and α_N values in this temperature range. The experimental values are listed in Table 1. The composite containing 64 wt.% natural graphite showed slightly larger average α_P value than the other composites. The composites α values were similar to reported literature values of nuclear graphite powders recorded in the temperature range 20-120 °C, i.e. 5.3×10^{-6} K^{-1} for isotropic graphites and for anisotropic graphites 2.2×10^{-6} K^{-1} with grain and 3.8×10^{-6} K^{-1} against grain [5]. Hacker et al. [6] also reported thermal expansion coefficients of extruded PGA graphite in this temperature range using dilatometry and obtained similar CTE values. For example, they reported that the average CTE in the direction parallel to extrusion direction was 2.5×10^{-6} K^{-1} while in the direction perpendicular to extrusion direction the average CTE value was 5.5×10^{-6} K^{-1}. The anisotropic ratio in expansion (α_P:α_N) in the temperature range 100-600 °C was greater than two for all the annealed composites. During pressing the flake-shaped graphite particles aligned normal to the pressing direction as shown by optical microscopy (see Figure 6). Therefore the enhanced

linear expansion in the pressing direction was caused by the expanding flakes during heat-treatment; on the other hand the composites expanded less in the direction normal to pressing.

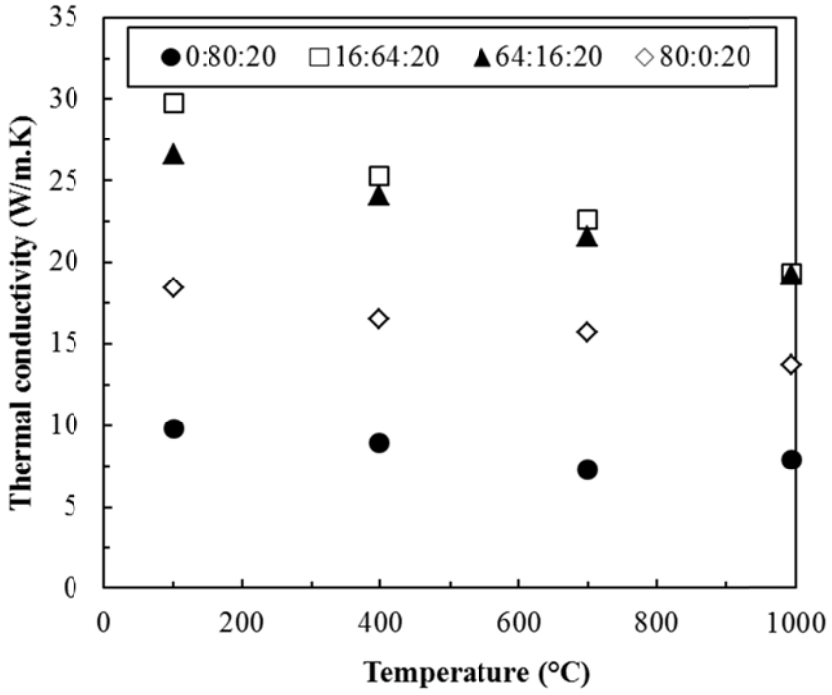

Figure 9: Temperature dependence of the thermal conductivity of the annealed graphite composites in the direction of pressing.

4.8 Thermal conductivity

The temperature dependence of thermal conductivity of the annealed graphite composites measured in the direction of pressing is shown in Figure 9. Generally the thermal conductivity values decreased with increasing temperature for all the annealed composites studied. This is because in graphite (the main component in the composites) heat conduction occurs mainly via lattice vibrations. As the temperature rises, phonon scattering becomes more pronounced and thus the thermal conductivities diminish [23, 24]. A composite containing only synthetic graphite and binder, i.e. 0 wt.% NG, showed lower values of thermal conductivity at a given measurement temperature. The thermal conductivity for this composite decreased from 9.8 $W.m^{-1}.K^{-1}$ at 100 °C to 7.9 $W.m^{-1}.K^{-1}$ at 1000 °C (i.e. a 19.4% decrease). The composite containing 16 wt.% NG showed higher thermal conductivities than other composites; it had a value of 29.8 $W.m^{-1}.K^{-1}$ at 100 °C and 19.3 $W.m^{-1}.K^{-1}$ at 1000 °C (35.4 % decrease). The composite containing 64 wt.% NG showed thermal conductivity values similar to those of 16 wt.% NG composite, i.e. 26.6 $W.m^{-1}.K^{-1}$ at 100 °C to 19.2 $W.m^{-}$

$^{1}.K^{-1}$ at 1000 °C (27.8 % decrease). The composite containing only natural graphite and binder showed values intermediate between the extremes; 18.4 to 13.7 $W.m^{-1}.K^{-1}$ at 100 and 1000 °C, respectively (decrease of 25.5 %). The contribution of the binder resin carbon to thermal conductivity values was very small since it had a very low thermal conductivity of ca. 0.3 $W.m^{-1}.K^{-1}$ at room temperature. In addition all the composites studied here contained the same amount of the binder resin and thus its influence should be the same. The composite containing only synthetic graphite and binder showed lower thermal conductivity values possibly for the following reasons:

- It had a higher open porosity than other composites (i.e. 41 %); this also evident from the polarised micrograph in Figure 6(a). It is well known that thermal conductivity decreases with increase in open porosity because heat transfer across pores is slow and inefficient [25].
- Since these composites are polycrystalline and it has been shown that a composite containing 0 wt.% NG had more structural disorder or defects than other composites (see XRD and Raman data), therefore the low thermal conductivity values could be due to phonon scattering effects at crystallite boundaries consistent with literature [23, 24].

The composites containing mainly natural graphite flakes were easily compactable compared to those containing synthetic graphite needle-like particles as evidenced by their high bulk densities. They also had larger aspect ratios, i.e. length: thickness ratio and therefore this is the reason why they conducted heat so well. This study found that the flakes orient themselves in the direction normal to pressing consistent with literature [26]. However the thermal conductivity values reported here were only obtained in the pressing direction due to sample geometry restrictions. It is expected that the thermal conductivity values in the direction transverse to pressing could be significantly higher than those attained in the pressing direction because of the fact that it will be in the direction of the flakes.

4.9 Flexural Strength

The four point bending flexural strength and modulus values for the annealed graphite composites measured in the pressing direction are listed in Table 1. The sample containing 40 wt.% NG featured a lower flexural strength and modulus than other composites. It is peculiar that the composite containing only synthetic graphite and binder with a higher porosity (i.e.

41 %) was much stronger. At this point an explanation cannot be offered but it might be related to differences in anisotropy caused by the uniaxial pressure applied during fabrication.

5 Conclusions

Model graphite-carbon composites were prepared by uniaxial cold compression moulding. They were prepared from mixtures of natural and synthetic graphite powders with a fixed amount (20 wt.%) of a phenolic novolac resin as binder. Optical microscopy showed that the natural graphite comprised flake-like particles while the synthetic one consisted of needle-like coke particles. The needle-coke particles were indistinguishable from the flakes on the micrographs of the annealed composites. The particles or flakes tended to align themselves normal to the pressing direction. The bulk density of the composites increased with increasing natural graphite content. Thermogravimetric analysis studies showed that the annealed graphite composites were stable in air up to 650 °C. The graphites used to make the composites were shown to have complimentary properties. The needle-like synthetic graphite was purer and more thermally stable. A composite of this graphite showed lower thermal expansion than composites containing mainly natural graphite. However, this composite also had a lower thermal conductivity in the temperature range 100 °C -1000 °C. On the other hand, the flake-like natural graphite was less pure and thermally less stable than the synthetic one. A composite made from this graphite had a larger thermal expansion coefficient than the one containing synthetic graphite. This composite showed slightly higher thermal conductivity values at than the composite containing only synthetic graphite. Anisotropy in properties was observed in these materials mainly due to the uniaxial compression employed during their preparation moulding which influenced particle alignment. It is interesting that composite containing 64 wt.% NG, with the highest anisotropy, featured the best mechanical properties.

Acknowledgements

This work is based upon research supported by the South African Research Chairs Initiative of the Department of Science and Technology and the National Research Foundation. Any opinion, findings and conclusions or recommendations expressed in this material are those of the authors and therefore the NRF and DST do not accept any liability with regard thereto. The PBMR and NECSA are thanked for financial support to P.P. Magampa and the provision of samples.

References

[1] D.R. Nicholls, The Pebble Bed Modular Reactor, Transactions of the Royal Society of South Africa, 56 (2001) 125-130.
[2] D.R. Nicholls, The Pebble Bed Modular Reactor, South African Journal of Science, 98 (2002) 31-35.
[3] C.H. Tang, Y. Tang, J.G. Zhu, Y.W. Zou, J.O. Li, X.O. Ni, Design and manufacture of the fuel element for 10 MW high temperature gas-cooled reactor, Nuclear Engineering and Design, 218 (2002) 91-102.
[4] H.S. Zhao, T.X. Liang, J. Zhang, J. He, Y.W. Zou, C.H. Tang, Manufacture and characteristics of spherical fuel elements for the HTR-10., Nuclear Engineering and Design, 236 (2006) 643-647.
[5] J.G. Cohn, E.W. Stern, S.F. Etris, Graphite, Artificial in: Kirk-Othmer (Ed.) Kirk-Othmer Encyclopedia of Chemical Technology, John Wiley & Sons, 2005, pp. 713-771.
[6] P.J. Hacker, G.B. Neighbour, B. McEnaney, The coefficient of thermal expansion of nuclear graphite with increasing thermal oxidation, Journal of Physics D: Applied Physics, 33 (2000) 991-998.
[7] L.M. Clark, R.E. Taylor, Radiation loss in the flash method for thermal diffusivity, Journal of Applied Physics, 46 (1975) 714-719.
[8] N. Cunningham, M. Lefevre, J.-P. Dodelet, Y. Thomas, S. Pelletier, Structural and mechanical characterization of as-compacted powder mixtures of graphite and phenolic resin, Carbon, 43 (2005) 3054-3066.
[9] P. Trucano, R. Chen, Nature, 258 (1975) 136.
[10] H. Lipson, A.R. Stokes, Procedings of the Physics Society of London, A181 (1942) 101.
[11] B.T. Kelly, Physics of Graphite, in, Applied Science Publishers, London and New Jersey, 1981.
[12] G. Parthasaray, B. Sreedhar, T.R.K. Chetty, Spectroscopic and X-ray diffraction studies on fluid deposited rhombohedral graphite from the Eastern Ghats mobile belt, India., Current Science, 90 (2006) 995-1000.
[13] W. Ruland, X-ray studies on the structure of graphitic carbons, Acta Crystallographica, 18 (1965) 992-996.
[14] F. Tuinstra, J.L. Koenig, Raman spectrum of Graphite, Journal of Chemical Physics, 53 (1970) 1126-1130.
[15] T.-H. Ko, W.-S. Kuo, Y.-H. Chang, Microstructural Changes of phenolic resin during pyrolysis, Journal of Applied Polymer Science, 81 (2001) 1084-1089.
[16] M. Nakamizo, R. Kammereck, J. P.L. Walker, Laser Raman studies on carbons, Carbon, 12 (1974) 259-267.
[17] I.A.S. Edwards, Structure in Carbons and Carbon Forms, in: H. Marsh (Ed.) Introduction to Carbon Science, Butterworths, London, 1989, pp. 1-36.
[18] M.E. Brown, Introduction to thermal analysis: techniques and Applications, Kluwer Academic Publishers, Dordrecht/ Boston/ London, 2001.
[19] H. Badenhorst, B. Rand, F.W. W., Modelling of natural graphite oxidation using thermal analysis techniques, Journal of Thermal Analysis and Calorimetry, 99 (2010) 211-228.
[20] N.J. Welham, J.S. Williams, Extended milling of graphite and activated carbon, Carbon, 36 (1998) 1309-1315.
[21] W. Jiang, G. Nadeau, K. Zaghib, K. Kinoshita, Thermal analysis of the oxidation of natural graphite-effect of particle size, Thermochimica Acta, 351 (2000) 85-93.
[22] T. Honda, T. Saito, Y. Horiguchi, Tanso, 72 (1972) 14.
[23] R. Taylor, K.E. Gilchrist, L.J. Poston, Thermal conductivity of polycrystalline graphite, Carbon, 6 (1968) 537-544.

[24] B.T. Kelly, K.E. Gilchrist, The basal thermal conductivity of highly oriented pyrolytic graphite as a function degree of graphitisation, Carbon, 7 (1969) 355-358.
[25] H. Matsuo, The effect of porosity on the thermal conductivity of nuclear graphite, Journal of Nuclear Materials, 89 (1980) 9-12.
[26] J.T. Mariner, H. Sayir, High thermal conductivity composite and method, in: U.s. Patent (Ed.), Advanced Ceramics Corporation, Lakewood, Ohio, United States of America, 1999.